nature neuroscience

A direct translaminar inhibitory circuit tunes cortical output

Scott Pluta[1,2], Alexander Naka[1,2], Julia Veit[1], Gregory Telian[1], Lucille Yao[1], Richard Hakim[1], David Taylor[1] & Hillel Adesnik[1]

Anatomical and physiological experiments have outlined a blueprint for the feedforward flow of activity in cortical circuits: signals are thought to propagate primarily from the middle cortical layer (layer 4, L4) up to L2/3 and down to the major cortical output layer (L5). Pharmacological manipulations, however, have contested this model and have suggested that L4 may not be critical for sensory responses of neurons in either superficial or deep layers. To address these conflicting models, we reversibly manipulated L4 activity in awake, behaving mice using cell type–specific optogenetics. In contrast with both prevailing models, we found that activity in L4 directly suppressed L5, in part by activating deep, fast-spiking inhibitory neurons. Our data suggest that the net effect of L4 activity is to sharpen the spatial representations of L5 neurons. Thus, we establish a previously unknown translaminar inhibitory circuit in the sensory cortex that acts to enhance the feature selectivity of cortical output.

The sensory neocortex is organized along its vertical axis into discrete layers[1,2]. A wealth of data characterizing the anatomy and synaptic connectivity of cortical neurons has implied the existence of a core circuit arranged vertically across these layers[3–7]. According to this model, thalamus drives L4, L4 drives L2/3 and L2/3 drives L5 (ref. 6). However, alternative synaptic pathways in the cortex, both local and long range, are known to exist, and evidence suggests that these alternative pathways might even be key drivers of cortical output, acting independently of L4 activity[8,9].

One recent study pharmacologically inactivated superficial cortical layers in sedated rats and found no effect on sensory responses in L5, suggesting a disconnect between the upper and lower layers of the cortex during sensory processing[9]. Other studies found that silencing L4 in the visual cortex of the anesthetized cat had no effect on the responses of the L2/3 neurons[8,10]. Precise latency analysis of sensory-evoked spikes in the rodent's barrel cortex also suggest a more complex picture than that proposed by the canonical circuit model[11]. However, no study has directly addressed these competing models using cell type–specific manipulations or in awake, behaving animals, a state in which cortical dynamics are known to be very different from anesthetized, sedated or non-alert conditions[12–14]. Thus, the neural circuits that govern the flow of sensory activity in the cortex under physiological conditions remain largely unresolved.

Using layer-specific optogenetic manipulation, we found that L4 activity in awake, behaving mice simultaneously drove L2/3 and suppressed responses in L5. The descending suppression of L5 was mediated by a direct, translaminar circuit in which L4 excitatory neurons drive fast-spiking (FS) inhibitory neurons in L5, a translaminar connection that has not been recognized previously. The functional consequence of this L4-to-L5 suppression was to sharpen sensory representations of L5 cortical projection neurons. This circuit was active in both somatosensory and visual cortex, suggesting that it may represent a conserved feature of the cortical circuit to improve sensory coding at the primary output stage of the neocortex.

RESULTS

Optogenetic suppression of L4 activity in awake, behaving mice

To directly assess the functional effect of L4 activity in a physiological context, we expressed the optogenetic silencer eNpHR3.0-YFP[15] in L4 excitatory neurons of the rodent somatosensory cortex using a Cre-dependent AAV vector[16] in scnn1-tg3-Cre[17] mice. In this strain, transgene expression was largely specific to excitatory neurons in L4, with the 'barrels' of rodent somatosensory cortex clearly visible (**Fig. 1a** and **Supplementary Fig. 1a**,**b**). Thus, we were able to use Cre-dependent AAV viral expression of optogenetic actuators in this Cre line to achieve specific manipulation of L4 activity.

We next devised an experimental preparation in which we could generate reproducible sensory-evoked responses in the barrel cortex of awake, behaving mice. Mice were head-fixed and habituated to running on a free-spinning circular treadmill (**Fig. 1b**). While running, mice rhythmically sweep their whiskers back and forth. This allowed us to present a tactile stimulus (a vertical bar) to different positions in the whisking field and drive reproducible, contact-evoked responses in the barrel cortex under conditions of active sensation (**Fig. 1c**)[12]. Neural activity was recorded with laminar silicon probes. We confirmed the laminar depth of electrodes on the silicon probe using a combination of approaches (**Supplementary Fig. 2**). This allowed us to assign each isolated unit to a specific layer in the barrel cortex

[1]Department of Molecular and Cell Biology and the Helen Wills Neuroscience Institute, University of California, Berkeley, California, USA. [2]These authors contributed equally to this work. Correspondence should be addressed to H.A. (hadesnik@berkeley.edu).

Received 15 July; accepted 31 August; published online 28 September 2015; doi:10.1038/nn.4123

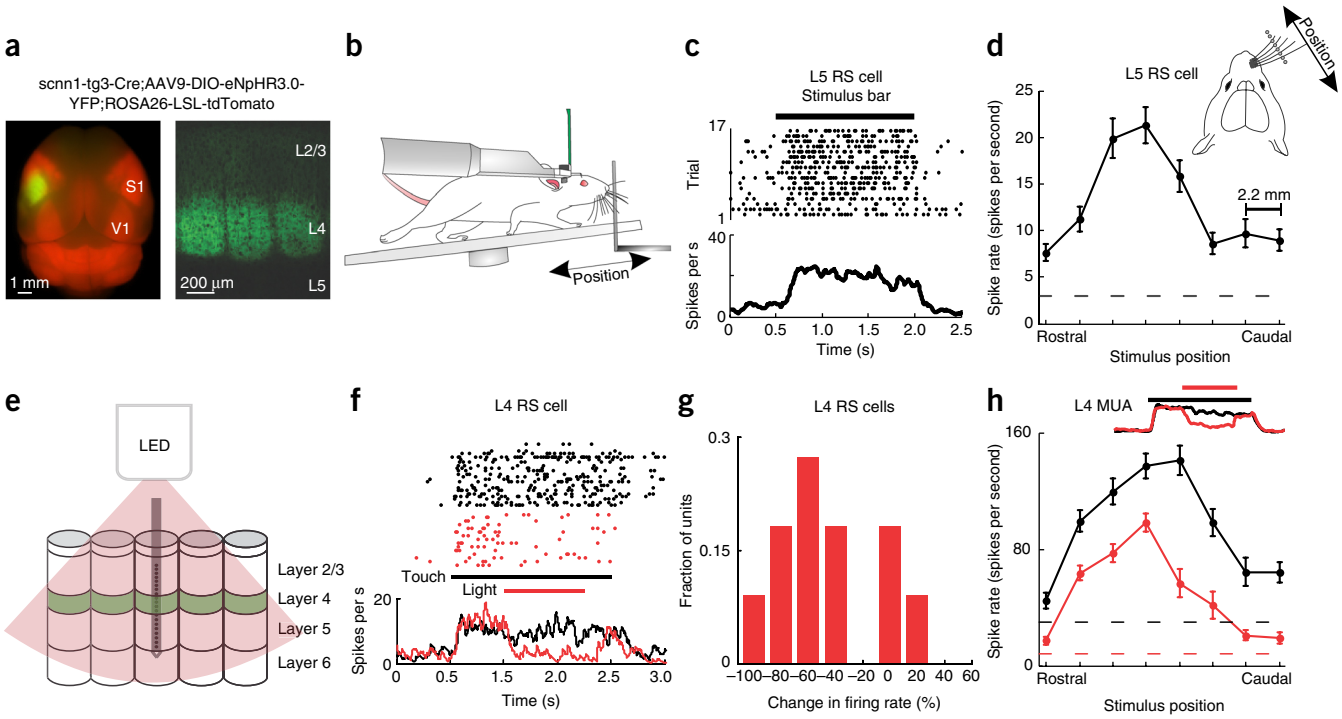

Figure 1 Optogenetic control of cortical L4 during active sensation. (**a**) Left, whole-brain epifluorescence image of the scnn1-tg3-Cre line crossed to a ROSA26-LSL-tdTomato reporter line. The left barrel cortex was injected with an eNpHR3.0-YFP Cre-dependent virus (yellow). Right, coronal section through the barrel cortex showing eNpHR3.0-YFP expression. (**b**) Schematic of the experimental configuration. A mouse was head-fixed on a free-spinning circular treadmill. A vertical bar moved by a stepper motor acted as a tactile stimulus. (**c**) Raster plot (top) and peri-stimulus time histogram (PSTH, bottom) of an isolated RS unit from L5 during presentation of the tactile stimulus. (**d**) Plot of firing rate versus stimulus position of the same L5 unit showing tuning to stimulus position. Dashed grain line indicates spontaneous firing in the absence of a stimulus. (**e**) Schematic of the optogenetic suppression of L4 neurons with light. (**f**) Raster plot (top) and PSTH (bottom) of an L4 RS unit that was suppressed by illumination of the cortex. Black line indicates the tactile stimulus; red line indicates the period of illumination. (**g**) Frequency histogram of the percent change in firing to the preferred stimulus of L4 RS units during illumination. Mean reduction in firing was 35 ± 14% ($P = 9.1 \times 10^{-6}$, $n = 11$ cells from 6 mice, two-way ANOVA, $f(1) = 21$). (**h**) PSTHs (top) and tuning curves (bottom) of multi-unit activity in L4 during illumination of the cortex. Dashed lines indicate average spontaneous firing rates during control (black) and illumination conditions (red). All error bars represent s.e.m.

(**Supplementary Fig. 2d**,**e**). We recorded units across multiple layers (L2–6), often in the same experiment.

We separated regular-spiking (RS) from FS cells[18] (Online Methods), with the former group largely representing excitatory cells, and the latter primarily corresponding to inhibitory neurons (although a subset of FS neurons may correspond to FS excitatory neurons[19]). Although L5 excitatory neurons can be separated into regular spiking and bursting subtypes[20], the majority of non-FS neurons in L5 showed a heterogeneous distribution of a tendency to spike in bursts (Online Methods) and were therefore considered as one group, referred to here as RS cells.

Under these conditions, cortical neurons showed sensory responses that were well tuned to the spatial position of the vertical bar, consistent with previous studies[21,22] (**Fig. 1d**). This tuning likely reflects a combination of the somatotopic organization of barrel cortex (which whiskers contact the bar at a given position) and information about the relative position of the whiskers at the time of contact with the stimulus[21,23]. At each position two to three whiskers contacted the stimulus bar, with 3–5 of 8 stimulus positions contacting the principal whisker. Nearby units, sorted off the same electrode, typically exhibited co-tuning for space, whereas the preferred spatial position of units varied across the whisker map (**Supplementary Fig. 2f**,**g**).

Illuminating the cortical surface with red light (30–80 mW, 1 mm optical fiber) reliably suppressed the activity of L4 units (**Fig. 1e**–**h**), demonstrating the effectiveness of our optogenetic approach. On a unit-by-unit basis, the majority (64%) of L4 RS units exhibited a significant reduction in firing during illumination (threshold $P < 0.05$, two-way ANOVA), whereas the remaining units showed no significant change (threshold $P > 0.05$, two-way ANOVA), perhaps reflecting incomplete infection of the eNpHR3.0 virus in L4 and/or incomplete penetrance of Cre expression.

The illumination area was set to suppress L4 across nearly all of barrel cortex. Notably, the same light level proportionally reduced L4 firing across all stimulus positions (**Supplementary Fig. 1c**), indicating that we could reduce L4 activity by the same fraction for both preferred and non-preferred stimuli. Illumination in control mice expressing only YFP had no significant effect ($P = 0.50$, $n = 16$ from 3 mice, $f(1) = 0.45$, two-way ANOVA; **Supplementary Fig. 3**). Moreover, suppressing L4 optogenetically did not result in changes in the kinematics of whisking (**Supplementary Fig. 4**). Thus, with this experimental system, we could reliably and specifically test the functional effect of L4 on cortical sensory activity in the absence of any changes in the sensory stimulus.

L4 drives L2/3, but suppresses L5

The major prediction of the conventional model of the neocortex is that inactivating L4 will reduce firing of neurons in L2/3 and L5, whereas the alternative models predict little or no effect on either L2/3 (ref. 8) or L5 (ref. 9). To address these contrasting notions, we

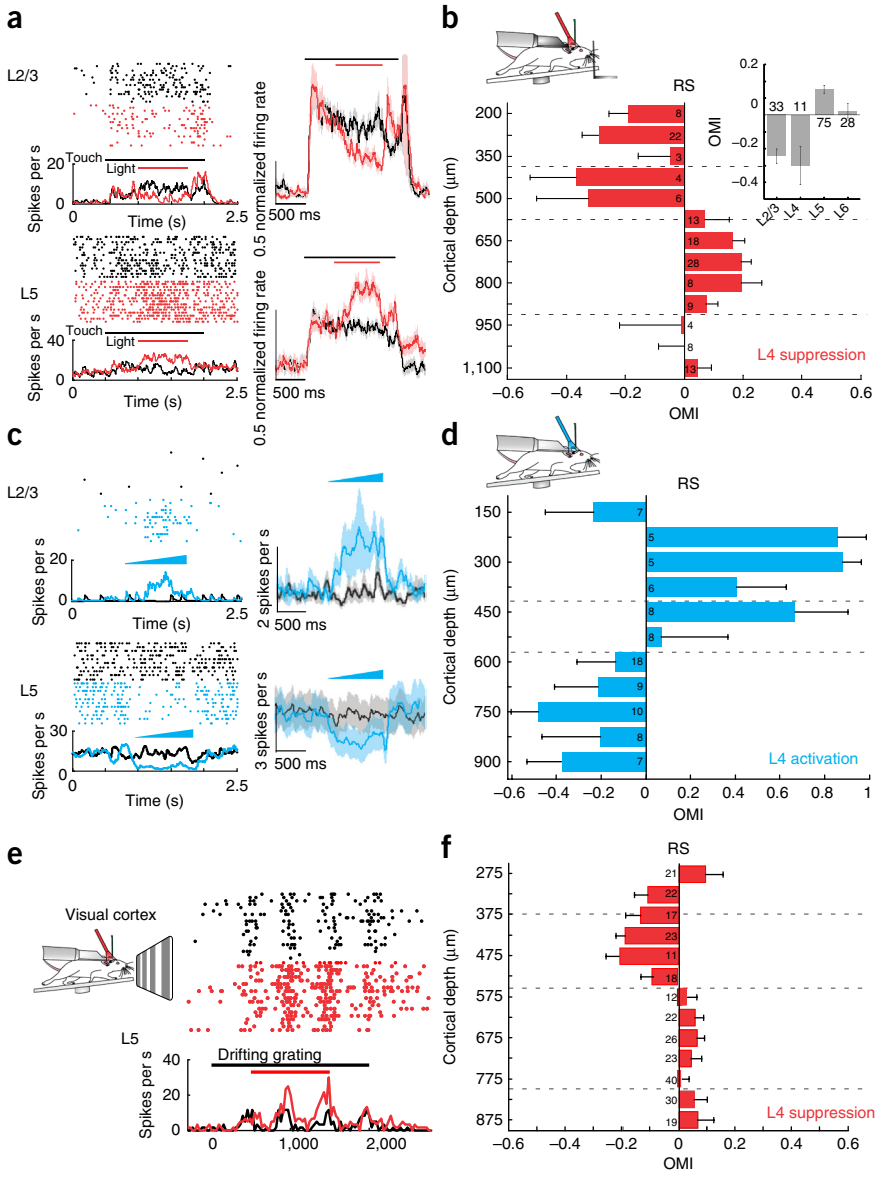

Figure 2 Optogenetic suppression of L4 deactivates L2/3 but facilitates L5. (**a**) Top left, raster plot (top) and PSTH (bottom) of a representative isolated L2/3 RS unit under control conditions (black) and during photo-suppression of L4 (red). Top right, population PSTH showing a reduction in evoked response ($P = 3.9 \times 10^{-6}$, $n = 33$ units from 5 mice, paired t test, $t(32) = 5.5$) of L2/3 RS units during suppression of L4. Bottom left, data presented as in top left for an L5 RS unit. Bottom right, population PSTH ($n = 75$) showing an enhancement in firing ($P < 10^{-6}$, $n = 75$ cells from 9 mice, two-way ANOVA, $f(1) = 27$) during suppression of L4. (**b**) Histogram of OMI during photo-suppression of L4 for all isolated RS units binned according to depth in the cortex. Each bin contains units spanning 25 µm above and below its marked center. (**c**,**d**) Data are presented as in **a** and **b** for photo-activation of L4 with ChR2 (L2/3, $P = 0.015$, $n = 19$ units from 3 mice, Wilcoxon signed rank test, $z = 2.4$; L4, $P = 0.0026$, $n = 20$ units from 3 mice, Wilcoxon signed rank test, $z = 3.0$; L5, $P = 0.046$, $n = 49$ units from 3 mice, Wilcoxon signed rank test, $z = 2.4$). Blue ramp indicates time of illumination. Shaded region indicates s.e.m. of firing rate. (**e**) Left, schematic of the recording configuration from visual cortex. Right, raster plot (top) and PSTH (bottom) for an example L5 RS unit during photo-suppression of L4 in V1 (red) and under control conditions (black). (**f**) Histogram of OMI versus cortical depth for all isolated RS units in V1 during photo-suppression of L4. L4: 24 ± 4.9% reduction in mean firing rate, $P < 10^{-6}$, $n = 59$ cells from 11 mice, Wilcoxon signed rank test, $z = 5.78$; L5: 14.2 ± 3.9% enhancement in mean firing rate, $P = 9.78 \times 10^{-5}$, $n = 123$ units from 11 mice, Wilcoxon signed rank test, $z = 3.9$. All error bars represent s.e.m.

optogenetically suppressed L4 while recording neuronal firing across the cortical layers. First, we focused on neurons in L2/3. We analyzed firing rates under both control and photo-suppression conditions at the steady-state portion of the sensory response (**Fig. 1**). Photo-hyperpolarizing L4 neurons resulted in a reduction in the sensory responses of L2/3 RS units (**Fig. 2a**). At their preferred stimulus position, the firing rates of L2/3 RS units were reduced by 39.3 ± 8% ($P = 3.9 \times 10^{-6}$, $n = 33$ cells from 5 mice, paired t test, $t(32) = 5.5$). This result confirms that L4 input is involved in driving L2/3 RS neuron activity and provides *in vivo* validation of one prediction of the conventional model of the neocortex.

We next focused on the functional effect of L4 suppression on L5 RS neurons. In contrast with all existing models of cortical function, we found that L4 photo-hyperpolarization enhanced L5 firing (**Fig. 2a**). On a unit-by-unit basis, 45 of 75 L5 RS cells exhibited a significant (threshold: $P < 0.05$, two-way ANOVA) light-induced enhancement during sensory stimulation. We computed an optogenetic modulation index (OMI, Online Methods) for each isolated unit that characterized how L4 photo-suppression affected its firing rate. A histogram of OMI (averaged across all conditions) versus cortical depth revealed that illumination of the cortex suppressed L4 and L2/3 (OMI < 0), but facilitated L5 (OMI > 0) (**Fig. 2b**).

Next we tested whether generating activity in L4, via expression of channelrhodopsin-2 (ChR2), would produce the opposite effects; namely, facilitating activity in L2/3 while suppressing L5. The light intensity was set so as to optogenetically generate firing rates in L4 neurons that were similar to what we observed physiologically (4.8 ± 1.6 Hz). Under these conditions, photo-activation of L4 facilitated the activity of L2/3 RS units (OMI: 0.37 ± 0.15, $n = 19$; **Fig. 2c**) while simultaneously suppressing activity in L5 (OMI: −0.27 ± 0.09, $n = 49$; **Fig. 2c**). A plot of OMI versus cortical depth quantified this effect across layers (**Fig. 2d**). Although optical stimulation cannot recapitulate the spatiotemporal characteristics of sensory drive, taken together with the previous experiments using photo-suppression, these results indicate that L4 activity is both necessary and sufficient to positively control neural activity in L2/3 while negatively controlling L5 responses.

To examine whether the L4-mediated suppression of L5 activity is a general feature of cortical circuits, we repeated the same experiment in mouse primary visual cortex (V1). Head-fixed, running mice were presented with drifting gratings at various orientations, sizes and contrasts (Online Methods). Photo-hyperpolarization of L4 neurons

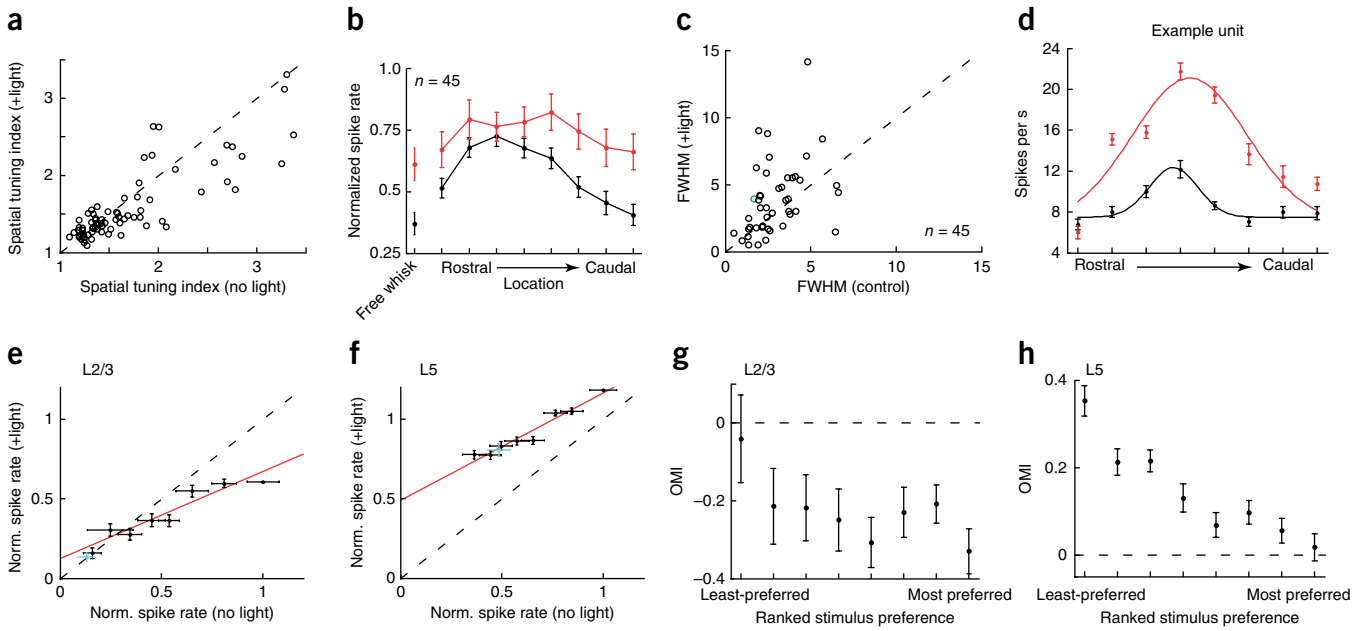

Figure 3 Suppression of L4 alters spatial tuning in L5. (**a**) Scatter plot of the spatial tuning index for L5 RS units during photo-suppression of L4 ($P = 0.003$, $n = 75$ units from 9 mice, paired t test, $t(74) = 3.1$). (**b**) Population average spatial tuning curve of L5 RS units under control (black) and during photo-suppression of L4 (red) for units showing significant tuning under control conditions ($n = 45$, $P < 0.001$, two-way ANOVA). The unconnected points are for the non-contact, free-whisking condition. (**c**) Scatter plot of the full-width half maximum of the Gaussian fit to well-fit spatial tuning curves of individual neurons during photo-suppression of L4 ($P = 0.016$, $n = 45$ units from 9 mice, Wilcoxon signed rank test, $z = 2.42$). (**d**) Example tuning curves with (red) and without (black) photo-suppression of L4. (**e**) Plot of the normalized spike rate under light versus control conditions in L2/3 RS units for rank-ordered stimulus preference ($n = 33$ units from 5 mice). The blue point indicates the control (non-contact) position. (**f**) Data are presented as in **c** for L5 RS units ($n = 75$ units from 9 mice). Blue dot indicates firing in the absence of a tactile stimulus (OMI: 0.23 ± 0.04, $P < 10^{-6}$, $n = 75$ units from 9 mice, Wilcoxon signed rank test, $z = 6.5$). (**g**) Plot of average OMI across L2/3 RS units as a function of rank-ordered stimulus preference ($P = 0.653$, $n = 33$ units from 5 mice, Kruskal-Wallis test, $\chi(7) = 5.0$). (**h**) OMI versus ranked stimulus preference for L5 RS units ($P < 10^{-6}$, $n = 75$ units from 9 mice, Kruskal-Wallis test, $\chi(7) = 82$). All error bars represent s.e.m.

in V1 had a similar effect of enhancing L5 activity for a wide range of stimuli (**Fig. 2e**,**f**). Illumination in control mice had no effect ($3.5 \pm 2.7\%$, $P = 0.82$, $n = 23$ units from 4 mice, Wilcoxon signed rank test, $z = -0.23$). Conversely, photo-stimulation of L4 in mice expressing ChR2 drove a significant suppression in the majority (24 of 45 units) of units in L5 (mean firing rate reduction: $55 \pm 5.7\%$, $P = 1.81 \times 10^{-5}$, $n = 24$ units from 3 mice, Wilcoxon signed rank test, z = 4.29). This suggests that suppression of L5 by L4 activity is likely to be a conserved feature across sensory cortical areas.

L4 sharpens sensory tuning in L5

How does the suppressive influence of L4 on L5 shape sensory representations? To address this question, we determined whether photo-hyperpolarizing L4 altered spatial tuning in L5 RS cells measured by presenting the stimulus bar in different locations along the horizontal axis. We computed a tuning index for each unit across the eight stimulus positions[24] (Online Methods). Photo-hyperpolarizing L4 broadened the representation of horizontal space across the population of L5 RS units (**Fig. 3a**,**b**). We also computed the width of each neuron's tuning curve (Online Methods) and found that, for units that were well fit by a Gaussian model (44 of 75 units, $r^2 > 0.75$), there was a strong and statistically significant increase in tuning width across the population ($P = 0.016$, $n = 45$ from 9 mice, $z = 2.42$, Wilcoxon sign-rank; **Fig. 3c**,**d**). This detuning could not be explained by a 'ceiling effect' on L5 firing. First, intrinsic limits on the spike rate of L5 excitatory neurons (measured with intracellular current injection in brain slices) readily exceed the average maximum firing rates observed *in vivo* (11.6 ± 1.2 Hz *in vivo* versus 42.4 ± 7.0 Hz *in vitro*). Second, L4 photo-suppression had no significant effect on the Fano factor of L5 RS cells ($P = 0.405$, $n = 75$ units from 9 mice, two-way ANOVA, $f(1) = 0.69$).

Do L4's effects on the spatial tuning of L5 neurons depend on surround interactions from other whiskers? To address this question, we optogenetically suppressed L4 in mice in which we trimmed all except the principal whisker (PW), restricting sensory activation to the PW's representation in the barrel cortex. Under these conditions, both the enhancement of L5 RS unit firing and the reduction of L5 FS unit firing persisted (**Supplementary Fig. 5d**,**e**). This indicates that these effects do not require surround whisker input and that they are mediated, at least in part, by descending circuits in the PW barrel column, although lateral inhibition from adjacent whisker representations may still contribute to the observed effects (see below).

To assess how L4 photo-suppression influenced stimulus-response functions of cortical neurons, we plotted the normalized firing rate of isolated units as a function of response magnitude for each stimulus. Photo-suppression of L4 scaled down the stimulus-response function of L2/3 RS units proportionally across all stimuli (**Fig. 3e**). In contrast, L4 suppression shifted stimulus-response functions of L5 RS units and drove a disproportionate enhancement for non-preferred stimuli (**Fig. 3f**).

To further examine how the effect of photo-suppression of L4 varies as a function of stimulus strength, we plotted OMI for each stimulus position versus stimulus preference (by rank-ordering stimuli from least to most preferred according to sensory-driven firing rate). For L2/3 units, there was a weak relationship between OMI and stimulus preference (**Fig. 3g**). In contrast, we observed a strong negative

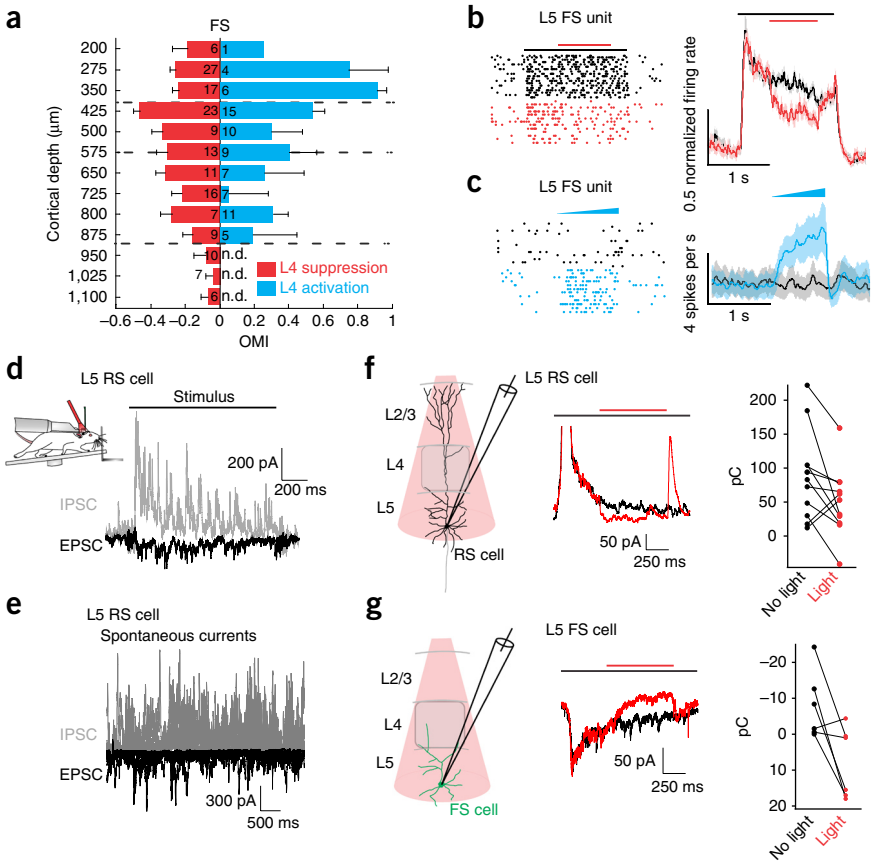

Figure 4 L4 drives FS neurons and synaptic inhibition in L5. (**a**) Histogram of OMI of FS units versus cortical depth for L4 photo-suppression (red bars) and L4 photo-activation (blue bars). (**b**) Representative example raster plot of an L5 FS unit (left) and population PSTH of L5 FS units (right) during L4 photo-suppression (red) or control conditions (black) (OMI: −0.25 ± 0.03, $P = 1.1 \times 10^{-6}$, $n = 53$ units from 9 mice, two-way ANOVA, $f(1) = 24$). Shaded region indicates s.e.m. of firing rate. (**c**) Data are presented as in **b** for photo-activation of L4 ($P = 0.001$, $n = 35$ units from 3 mice, Wilcoxon signed rank test, $z = 3.4$). (**d**) Example traces of synaptic excitation (black) and inhibition (gray) recorded in whole-cell voltage-clamp mode from a L5 neuron during tactile stimulation in head-fixed, locomoting mice. (**e**) Example traces of synaptic excitation (black) and inhibition (gray) during locomotion, but in the absence of any external tactile stimulus. (**f**) Left, schematic of the recording configuration from L5 putative RS cells. Middle, average traces of synaptic inhibition under control conditions (black) or during L4 photo-suppression for all recorded L5 RS cells. Right, plot of net inhibitory synaptic charge in L5 neurons under control conditions (black points) or during photo-suppression of L4 (red points, $n = 11$ cells in 9 mice, $P = 0.048$, paired t test, $t(10) = 2.2$). (**g**) Left, schematic of the recording configuration from L5 putative FS cells. Middle, average traces of synaptic excitation for all putative L5 FS cells under control conditions (black) or during L4 photo-suppression. Right, plot of net excitatory synaptic charge in putative L5 FS cells under control conditions (black points) or during photo-suppression of L4 (red points) ($n = 6$ cells in 5 mice, $P = 0.035$, paired t test, $t(5) = -2.9$). All error bars represent s.e.m.

relationship for L5 units, with OMI sloping toward zero for the most preferred stimuli (**Fig. 3h**).

On a unit-by-unit basis in L5, OMI was significantly larger for the least preferred stimulus position, as compared with the most preferred ($P < 10^{-6}$, $n = 75$ from 9 mice, $t(74) = 8{,}2$, paired t test; **Supplementary Fig. 5a**). In addition, 77% (58 of 75) of L5 units exhibited a negative correlation (mean $r^2 = -0.33$) between stimulus preference and the absolute number of spikes added by L4 photo-suppression. Thus, L4 photo-suppression disproportionally enhanced L5 RS neuron firing for non-preferred stimuli (**Supplementary Fig. 5b**,**c**), broadening the spatial tuning of the L5 RS population as a consequence (**Fig. 3b**). These results indicate that the normal role of L4 is to sharpen sensory representations of L5 cortical neurons.

Although we analyzed how neurons are tuned for space, the suppressive action of L4 on L5 persisted even in the absence of external contact with the stimulus bar (**Fig. 3f**), indicating that even ongoing activity in L5 is under tonic suppressive control by L4 output ($P < 10^{-6}$, $n = 75$ from 9 mice, Wilcoxon sign-rank, $z = 6.5$). Thus, L4 may generally sharpen L5 neurons' sensory tuning by reducing spontaneous activity and suppressing responses to non-optimal stimuli.

L4 drives synaptic inhibition in L5

What could account for the suppressive action of L4 on L5 activity? L4 is known to drive both feed-forward[25] and recurrent[26] inhibition through FS interneurons in the superficial cortical layers. Thus, we tested whether L4 might also drive FS inhibitory neurons *in vivo*, which could potentially account for an important component of the suppression of L5 RS neurons. During photo-suppression of L4 (as above), we observed a pronounced reduction in FS neuron firing rates across layers, including FS units in L5 (OMI, −0.25 ± 0.03), computed as a negative OMI across all cortical depths (**Fig. 4a**,**b** and **Supplementary Fig. 6**). Although the largest percent reduction in FS unit firing was in L4 (−52 ± 3%, $n = 35$ units from 6 mice), strong reductions were also observed both for L5 (−30 ± 5%, $n = 53$ units from 9 mice) and L2/3 (−31 ± 3, $n = 50$ units from 5 mice) FS units, with the largest absolute reduction in firing rate observed in L5 FS units (**Supplementary Fig. 6**). FS units in L6 were not significantly affected ($P = 0.55$, $n = 25$ from 3 mice, two-way ANOVA, $f(1) = 0.36$), suggesting that L4 activity does not substantially influence inhibition originating from L6 FS units[27] (**Supplementary Fig. 6**). Conversely, photo-activation of L4 increased the firing rate of most FS neurons outside of L6 (mean rate increase: 3.9 ± 0.43 Hz, mean OMI: 0.39 ± 0.05; **Fig. 4a**,**c** and **Supplementary Fig. 6**). Thus, activity in L4 RS neurons is both necessary and sufficient to drive a component of the activity of FS neurons in L2/3, L4, and L5.

These results implicate FS interneurons as possible mediators of L5 suppression. Thus, we hypothesized that L4 suppresses L5 by driving interneurons that inhibit L5 RS cells. If so, photo-suppressing L4 should reduce sensory-evoked synaptic inhibition in L5 RS cells. To test this idea, we measured synaptic currents from L5 neurons using whole-cell patch-clamp recordings in the same conditions as described above; namely, head-fixed, but freely locomoting mice. First, we established a stabilized preparation so that neurons could be recorded in the whole-cell voltage-clamp mode for prolonged

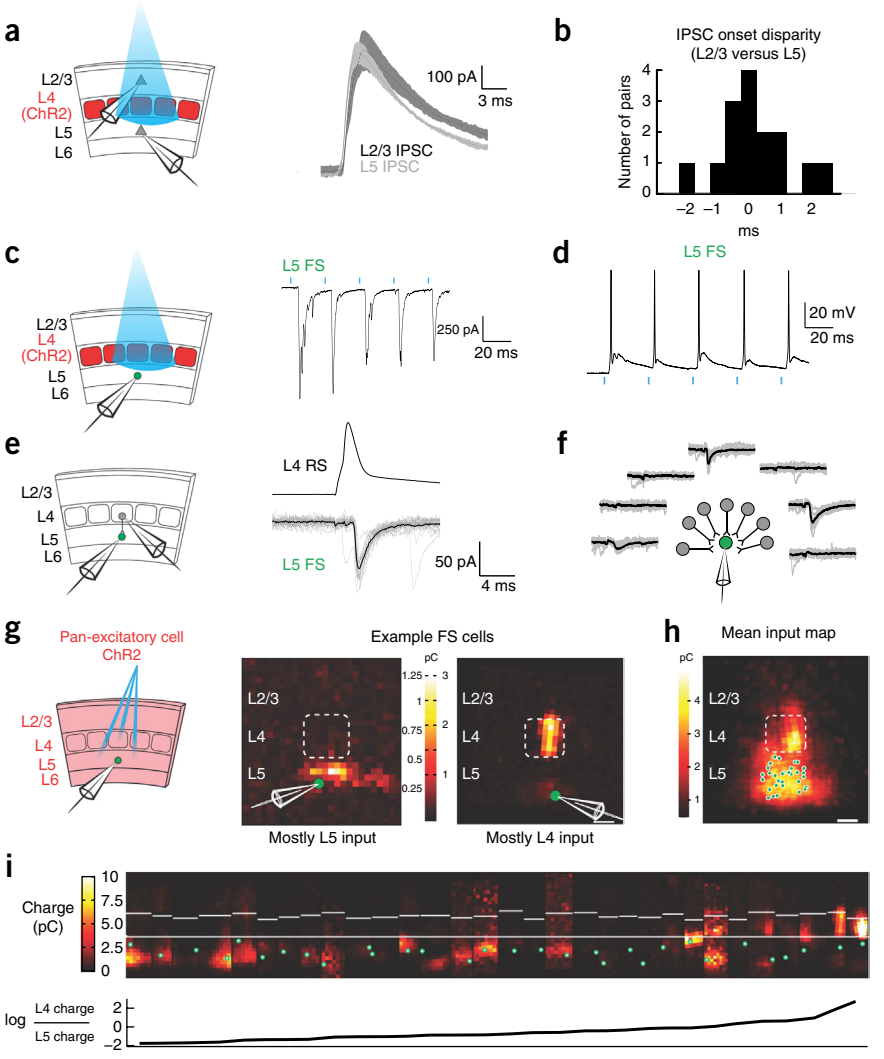

Figure 5 Mapping a direct translaminar inhibitory circuit from L4 to L5 via L5 FS cells. (**a**) Left, recording schematic of a pair of simultaneously recorded L2/3 and L5 pyramidal cells in mice expressing ChR2 in L4. Right, example traces of light evoked synaptic inhibition in a L2/3 (dark gray) and a L5 (light gray) pyramidal cell. (**b**) Histogram of the difference in mean onset latency of light evoked synaptic inhibition in simultaneously recorded pairs of L2/3 and L5 neurons (L2/3, 4.9 ± 0.4 ms; L5, 4.7 ± 0.4 ms; $P = 0.49$, $n = 13$ pairs in 10 slices from 5 mice, paired t test, $t(12) = 0.70$). (**c**) Left, recording schematic of an intracellularly recorded L5 FS neuron in mice expressing ChR2 in L4. Right, example traces of light-evoked synaptic excitation in a L5 FS neuron. Blue lines indicate 1-ms pulses of blue light. (**d**) Example trace of the first five synaptically evoked action potentials in a L5 FS neuron during a train of photo-stimulation of L4. (**e**) Left, recording schematic of a simultaneously recorded L4 excitatory cell and a L5 FS neuron. Right, example traces of an evoked action potential in the L4 excitatory neuron (top trace) and unitary excitatory postsynaptic currents (EPSCs, gray, single trials; black, average) in a connected L5 FS neuron. (**f**) Schematic of an example recording in which seven candidate presynaptic L4 excitatory neurons were recorded in a pair with a L5 FS neuron. (**g**) Left, recording schematic of a digital-micromirror based optogenetic mapping system in emx1-IRES-Cre mice injected with a flexed-ChR2 AAV vector. Right, two example excitatory input maps from FS neurons exhibiting mostly L5 input (left) or mostly L4 input (right). Scale bar represents 100 µm. (**h**) The grand average excitatory input map from all recorded L5 FS neurons ($n = 31$ FS cells in 26 slices from 13 mice), aligned by the position of the L4 barrel above each neuron. Green dots indicate the location of the somata of the recorded FS neurons. Scale bar represents 100 µm. (**i**) All individual excitatory input maps recorded in L5 FS neurons. Green dots indicate the location of the somata of the recorded FS neurons. White lines indicate the top and bottom boundaries of L4. Bottom, maps from the recorded FS cells are rank-ordered according to the L4:L5 ratio of home column input (quantified as mean charge transfer per unit area). All error bars represent s.e.m.

periods and with low access resistances (Online Methods) to better estimate excitatory and inhibitory currents. As the mouse actively contacted the stimulus bar with its whiskers, we observed barrages of excitatory and inhibitory synaptic inputs (**Fig. 4d**). Spontaneous excitation and inhibition exhibited an average ratio of ~1:2 (mean excitatory charge = 56 ± 2 pC s^{-1}; mean inhibitory charge = 100 ± 0.07 pC s^{-1}, $n = 11$ cells in 9 mice; **Fig. 4e**). Thus, L5 neurons were under a tonic inhibitory drive, consistent with the spontaneous firing rates of FS units we observed during extracellular recording (3.3 ± 0.6 Hz in L5 FS cells, $n = 53$). During sensory stimulation, when FS units showed a marked increase in their firing rate, photo-hyperpolarizing L4 excitatory neurons resulted in a significant reduction in evoked inhibitory input to L5 RS neurons, sometimes reducing it to below baseline levels (control: 117 ± 25 pC; light: 67 ± 20 pC, $n = 11$, $P < 0.04$; **Fig. 4f**). In contrast, we observed no significant change in synaptic excitation (control: 40 ± 5 pC; light: 65 ± 25 pC, $n = 12$, $P = 0.49$), even though L4 excitatory neurons are known to monosynaptically innervate L5 pyramidal cells[28]. This lack of change in excitatory drive in L5 RS neurons during L4 suppression may be explained by the increased recruitment of recurrent excitatory inputs from within L5 (ref. 29), as L4 suppression enhances L5 RS unit firing. These results demonstrate that L4 activity is responsible for a substantial component of the synaptic inhibition in L5 neurons.

How might L4 generate inhibition in L5? Our extracellular recordings suggest that L4 could drive spiking in FS cells, which then inhibit L5 RS neurons. We hypothesized that L5 FS cells in particular might be a primary mediator, as these cells are known to densely target L5 pyramidal cells[30–32]. If L4 generates inhibition in L5 through L5 FS cells, then L4 photo-suppression should reduce excitatory input in L5 FS cells. We addressed this by analyzing a subset of the L5 neurons that we recorded in whole-cell mode *in vivo* that we categorized as putative FS (pFS) neurons on the basis of their intrinsic synaptic properties, a classification we could confirm by comparing such measurements from positively identified FS neurons in brain slices, and for a subset of neurons *in vivo* in which we collected action potentials in the cell-attached or current-clamp mode before voltage clamping (**Supplementary Fig. 7** and Online Methods). When we optogenetically hyperpolarized L4 excitatory neurons, we observed a pro-

nounced reduction in their excitatory input, and in five of six cells the time-averaged excitatory charge was reduced to below baseline levels (average OMI: 2.4 ± 1.0; control: −8 ± 4C, light: 8 ± 4 pC, $P = 0.035$, $n = 6$; **Fig. 4g**). Notably, although synaptic inhibition in L5 cells dropped rapidly following the onset of light, excitation to pFS neurons decayed more slowly. This may be explained by the non-linearity imposed by the action potential threshold in L5 FS cells, such that even a partial drop in their excitatory input can markedly reduce their firing rate, and thus their inhibitory output. These results suggest that L4 activity drives excitation in L5 pFS neurons, which is consistent with the reduced firing of L5 FS neurons during L4 photo-suppression.

A direct feedforward inhibitory circuit from L4 to L5

These results suggest a possible circuit to account for the suppressive influence of L4 on L5: L4 might directly recruit L5 inhibitory neurons, generating disynaptic somatic inhibition in L5 pyramidal cells. Although it is well known that L4 excitatory neurons synapse on L5 pyramidal cells[28], to our knowledge, the direct L4 innervation of L5 inhibitory neurons has never before been observed. Thus, we sought to verify its existence using acute brain slices from the barrel cortex. Photo-stimulation of L4 *in vitro* resulted in fast excitatory and inhibitory currents in both L2/3 and L5 pyramidal cells (**Fig. 5a**). The observed inhibition was almost entirely abolished by glutamatergic antagonists (**Supplementary Fig. 1d**), demonstrating that it was mediated by synaptic recruitment of inhibitory interneurons. The onset latencies of inhibition in L2/3 and L5 pyramidal cells showed no significant difference ($P = 0.49$; **Fig. 5b**), indicating that L4 might directly activate inhibitory neurons that suppress L5, and not operate poly-synaptically through L2/3 pyramidal cells (**Fig. 6**).

To address the existence of a direct circuit linking L4 and L5 FS neurons, we first made whole-cell recordings from electrophysiologically identified FS neurons in L5 (Online Methods). Photo-stimulation of L4 resulted in large, short-latency (mean: 3.77 ± 0.48 ms) excitatory synaptic currents, and in most cases reliably drove action potentials in the recorded L5 FS neurons (8 of 14 cells; **Fig. 5c**,**d**). To demonstrate directly that this is a monosynaptic connection, we made paired intracellular recordings from L4 excitatory neurons and L5 parvalbumin (PV)$^+$ FS neurons (labeled in the PV-Cre; ROSA-LSL-tdTomato line) located in the same barrel column. Of a total of 55 tested connections, we observed nine positive connections with an average unitary conductance of 0.66 ± 0.10 nS (**Fig. 5e**) on the first presynaptic action potential. This is comparable to the connectivity rate observed between L4 and L2/3 FS cells[25]. When we restricted our estimate of connection probability to postsynaptic PV$^+$ FS cells showing at least one monosynaptic connection with an excitatory neuron in L4, connection probability rose to 39% (9 of 23 connections). In one L5 PV$^+$ FS cell, three of seven tested connections were positive (**Fig. 5f**). This result suggests that L4 neurons may preferentially innervate a subset of L5 PV cells.

To estimate the laminar pattern of intracortical excitatory connectivity onto L5 inhibitory neurons, we used a digital micromirror device (DMD) to spatially control optogenetic photo-stimulation and mapped the excitatory input to L5 FS neurons across barrel columns and cortical layers (**Fig. 5g**). ChR2 was expressed in excitatory neurons throughout the cortex using the emx1-Cre line[33]. ChR2-expressing neurons were photo-activated primarily within 50 µm of the illumination spot, ensuring sublaminar spatial resolution (**Supplementary Fig. 8a–d**). Illumination was specifically chosen to limit polysynaptic activity and prevent activation of axons of passage (Online Methods). Although all L5 FS neurons

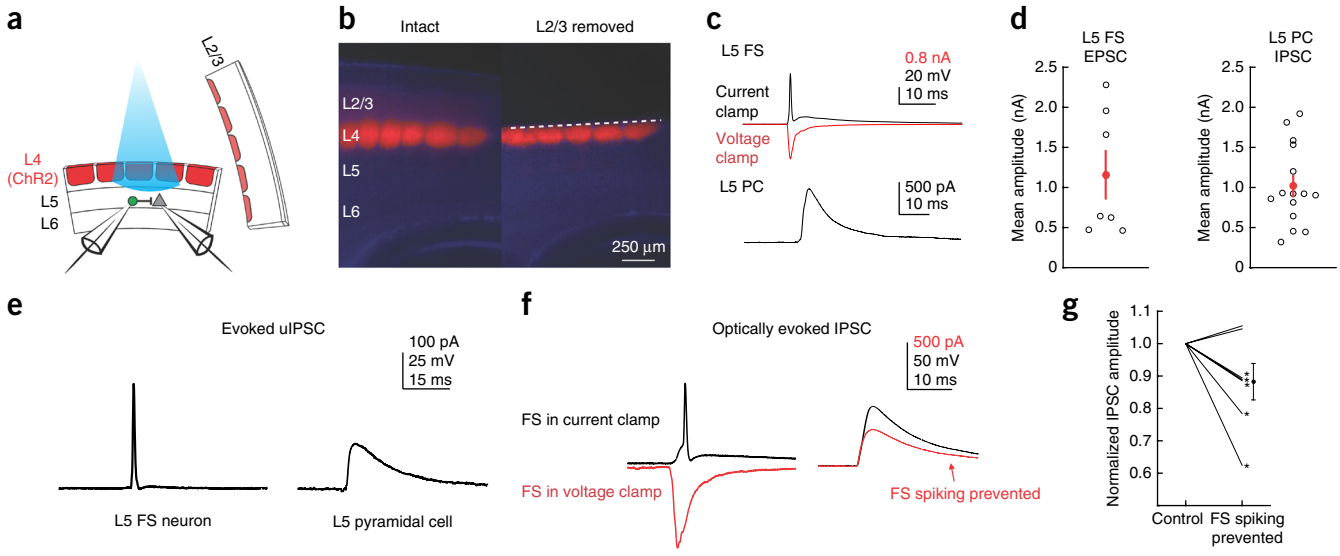

Figure 6 L4-to-L5 translaminar inhibition through L5 FS neurons persists in the absence of L2/3. (**a**) Recording schematic. L2/3 is surgically removed from the brain slice, and a paired recording is made from a L5 FS and a L5 pyramidal cell. (**b**) Example images from an intact slice expressing ChR2-TdTomato in L4 (left) and a slice with L2/3 surgically removed (right). (**c**) Top, example average light-evoked response recorded in a L5 FS neuron after removal of L2/3. Black, current clamp; red, voltage clamp. Bottom, evoked IPSC in a L5 pyramidal cell. (**d**) Scatter plot of the mean amplitude of the evoked EPSCs in L5 FS cells (left, $n = 7$ cells in 7 slices from 3 mice) and of IPSCs in L5 pyramidal cells (PC, right, $n = 15$ cells in 12 slices from 3 mice). (**e**) Left, action potential evoked by current injection in a connected L5 FS-L5 PC pair. Right, unitary IPSC recorded in the postsynaptic pyramidal cell. (**f**) Same pair as shown in **e**. Left, optically evoked response of the L5 FS in current clamp (black) and during voltage clamp (red). Right, optically evoked IPSC in the L5 pyramidal cell when the FS cell is allowed to spike (black) or prevented from spiking (red). (**g**) Scatter plot of the mean change in the optically evoked IPSC in the L5 pyramidal cell when the presynaptic L5 FS cell is prevented from spiking by voltage clamping. $^*P < 0.05$ (range: $P = 10^{-12}$ to 0.21, $n = 7$ pairs in 5 slices from 3 mice t test). All error bars represent s.e.m.

received some excitatory input from L5 (**Fig. 5h** and **Supplementary Fig. 8e–i**), ~23% (7 of 31) received their densest excitatory input from L4 of the same barrel column (**Fig. 5h** and **Supplementary Fig. 8i**), consistent with paired recordings.

Next, to test whether L2/3 was dispensable *in vitro* for L4-generated inhibition in L5 pyramidal cells, we surgically removed L2/3 entirely. In these slices, even in the complete absence of L2/3, we observed that photo-stimulation of L4 was still sufficient to generate disynaptic inhibition in L5 pyramidal cells (**Fig. 6a–c**). This result demonstrates that neither excitatory nor inhibitory cells in L2/3 are required for L4 to drive inhibition in L5. Given that this transection also severs the apical dendrites of L5 pyramids, it further indicates that the remaining inhibition is either somatic or targeted to L5 neurons' proximal dendrites.

To support the notion that L4 activates L5 FS cells directly, which in turn generates synaptic inhibition in L5, we made paired recordings from connected L5 FS and L5 pyramidal cells while photo-stimulating L4. As described above, light pulses to L4 drove firing in L5 FS cells and generated inhibitory currents in L5 pyramidal cells. When we prevented the synaptic activation of the recorded L5 FS cell by holding it in voltage clamp, we observed a significant (threshold = $P < 0.05$) and reversible reduction in the photo-induced inhibitory postsynaptic current (IPSC) in the L5 pyramidal cell in 5/7 connected pairs (mean reduction = 12 ± 6%; **Fig. 6e,f**).

Contributions to L5 suppression by other inhibitory circuits

Taken together, these results establish a direct translaminar inhibitory circuit connecting L4 with L5 pyramidal cells via FS inhibitory neurons. Nevertheless, other intracortical circuits likely contribute to L4's ability to suppress L5 excitatory neurons, including FS neurons in other layers, polysynaptic recruitment of L5 FS neurons through L2/3 pyramidal cells and non-FS inhibitory neurons. Thus, we sought to systematically test whether each of these other possibilities might contribute to L4-to-L5 translaminar suppression.

Given that photo-suppressing L4 neurons reduced FS neuron firing rates across L2/3–5, we quantitatively measured the relative strength of inhibitory input onto L5 pyramidal cells from FS neurons in different layers to address their potential relative contributions to translaminar inhibition. We expressed ChR2 selectively in PV^+ inhibitory neurons using the PV-Cre line and used the same DMD-based mapping approach described above (**Supplementary Fig. 9**). Consistent with previous studies[34,35], L5 pyramidal cells received the majority of their monosynaptic PV^+ mediated–inhibition from PV cells in L5 (>70% of total charge transfer; **Supplementary Fig. 9a,b,e**). Taken together with the finding that L5 FS cells also display the largest absolute decrease in firing rate during L4 photo-suppression, this suggests that the majority of FS-mediated L4 to L5 inhibition is routed through FS cells in L5.

Next we asked whether L5 FS neurons might be recruited polysynaptically through L2/3 excitatory neurons. To address this question, we optogenetically suppressed L2/3 excitatory neurons *in vivo* using the drd3-Cre driver line[36], which labels L2/3 pyramidal cell in the barrel cortex (**Supplementary Fig. 10a**). Despite a pronounced suppression of L2/3 excitatory neurons, L5 FS neurons as a population were not significantly reduced ($P = 0.45$, $n = 74$ from 7 mice, $f(1) = 0.69$, two-way ANOVA), in contrast with when we photo-suppressed L4 (**Supplementary Fig. 10b**). The lack of a consistent effect on L5 FS cells is in agreement with reports that L2/3 pyramidal cells in agranular cortex selectively excite L5 SOM^+ and not L5 PV^+ neurons[37,38]. This experiment suggests that the decrease in L2/3 activity during L4 photo-suppression probably only makes a minor contribution to the disinhibition of L5 neurons through FS cells. However, we cannot rule out a contribution from L2/3 that operates independently of FS neurons.

Finally, we asked whether non-FS GABAergic interneurons could significantly contribute to the L4-mediated suppression of L5 excitatory cells. We addressed this possibility in two ways. First, we asked whether L4 excitatory neurons also monosynaptically innervate L5 SOM^+ Martinotti cells. We made paired intracellular recordings from L4 excitatory neurons and GFP^+ neurons in the GIN line, which exclusively labels SOM^+ Martinotti cells[39,40]. In contrast with the frequent connectivity onto L5 PV^+ neurons, we never observed direct connections from L4 excitatory neurons onto GFP^+ cells in the GIN line (52 connections tested onto 18 L5 GIN GFP^+ cells, 0 of 18 L5 GIN GFP^+ versus 5 of 12 L5 PV^+/FS received at least one monosynaptic connection, $P = 0.0056$, Fisher's exact test, DF = 1), likely excluding them from being directly involved in the L4-to-L5 translaminar suppressive circuit. Next, we asked whether photo-suppressing L4 *in vivo* results in an increase in the burst rate of L5 neurons, as would be expected for a reduction in dendritic inhibition[41]. However, we found that despite robustly increasing L5 RS unit firing rates, L4 suppression did not lead to a significant increase in the tendency of L5 RS units to fire spikes in bursts in S1 or V1 (S1: $P = 0.67$, $n = 74$ from 9 mice, Wilcoxon sign-rank; V1: $P = 0.69$, $n = 123$ from 11 mice, Wilcoxon sign-rank; **Supplementary Fig. 11a–e**). As a positive control, directly suppressing SOM^+ neurons (by expression of eNpHR3.0 in SOM-Cre mice) increased the tendency of L5 neurons to burst (**Supplementary Fig. 11g,h**). Although other inhibitory circuits are likely to contribute, these three lines of experiments lend additional support to the model that L4 excitatory neurons monosynaptically drive L5 FS neurons, which in turn potently suppress L5 excitatory neurons during sensory stimulation.

DISCUSSION

Our findings reveal a previously unknown translaminar inhibitory circuit that directly connects the input and output layers of the cortex. The functional consequence of this circuit is to enhance the feature selectivity of cortical output. More generally, our results lead us to rethink the nature of signal propagation in neocortical circuits. On the one hand, anatomical and physiological data support the notion of a simple feedforward excitatory circuit in which L4 drives L2/3 and L2/3 drives L5. On the other hand, pharmacological manipulations in anesthetized or sedated animals suggest that L4 activity may not be required for sensory responses in L2/3 or in L5. Our data support a new model to more accurately describe functional interactions in the cortex during sensory processing in behaving animals. Consistent with a previously described model[9], we found that L4 activity is not required for sensory responses in L5. In contrast with this model, we found that L4 actually exerts an inhibitory effect on L5 activity. This might have been missed previously owing to the exceptionally low firing rates of superficial cortical neurons in sedated animals[9], the strong adaptation of intracortical activity during passive conditions[42,43] or the absence of a neuromodulator that is only present during active brain states, rendering this suppressive mechanism inactive under these reduced states and only detectable in awake, behaving animals.

With respect to signal propagation to L2/3, our results are consistent with the more conventional model, as we found that L4 is involved in driving L2/3 in response to sensory stimuli. However, we cannot rule out the involvement of cortical feedback from other areas, such as secondary somatosensory cortex or primary motor cortex, which may explain, in part, the incomplete deactivation of L2/3 when photo-

suppressing L4. Taken together, our results suggest a revised model of signal flow through the cortical layers: sensory input propagating through L4 drives L2/3 while simultaneously suppressing L5 through disynaptic inhibition.

Our results suggest that L4 to L5 suppression can be attributed, at least in part, to a previously unrecognized circuit in which L4 excitatory neurons directly activate a subpopulation of FS inhibitory neurons in L5, which in turn suppress L5 projection neurons and sharpen their sensory representations. This model is supported by several lines of evidence based on the optogenetic suppression and activation of L4 excitatory neurons *in vivo* and in brain slices. Although we provide data that L5 Martinotti cells and FS cells in other layers are not likely to substantially contribute to the translaminar inhibitory circuitry that we studied, other inhibitory circuits that we did not directly examine could also contribute. For example, other subtypes of cortical inhibitory interneurons that target L5 pyramidal cells[44,45], including SOM$^+$ non-Martinotti cells[39] and non-FS inhibitory neurons in more superficial layers, may receive excitatory input from L4 and could provide alternative sources of translaminar inhibition. These will be important questions to address in the future.

Notably, we observed that L4-to-L5 translaminar suppression disproportionally affects non-preferred stimuli. Thus, the net effect of this suppression is to sharpen sensory tuning curves, in this case for horizontal space. This suppression is likely a result of an increase in inhibition from FS inhibitory neurons, which, when combined with the nonlinearity of action potential threshold in L5 pyramidal cells, preferentially suppresses pyramidal cells' responses to non-optimal stimuli[46]. We note that we observed changes in spatial tuning in both S1 and V1, which is akin to a broadening of their spatial receptive fields.

There is ample evidence that inhibitory circuits control tuning in the somatosensory cortex[24,47] and in other cortical areas[48–50]. Unlike other inhibitory circuits that have been proposed to enhance tuning to specific stimulus features, the L4-to-L5 inhibitory circuit that we describe here might generally enhance tuning to multiple sensory features, not just for space. This notion is supported by the fact that L4 suppresses L5 even when no external stimulus is present. By reducing a component of the ongoing or 'non-sensory' firing of L5 projection neurons, the L4-to-L5 translaminar inhibitory circuit should enhance the relative modulation of cortical neurons to all sensory stimuli.

Furthermore, given that we observed this suppression in both somatosensory and visual cortices, this mechanism might generally improve coding at the output level of the cortex in many cortical areas. It will be interesting to determine whether the synaptic connection between L4 excitatory neurons and L5 interneurons is controlled by higher cortical areas. If so, it might represent a key node for dynamically sharpening stimulus representations in different brain states or under different behavioral demands.

METHODS

Methods and any associated references are available in the online version of the paper.

Note: Any Supplementary Information and Source Data files are available in the online version of the paper.

ACKNOWLEDGMENTS

We are grateful to K. Deisseroth (Stanford University) and S. Sternson (Janelia Farms Research Campus, HHMI) for optogenetic reagents and to D. Kleinfeld (University of California, San Diego) for spike sorting software. This work was supported by National Institute of Neurological Disorders and Stroke grant DP2NS087725-01 and National Eye Institute grant R01EY023756-01, and a Whitehall foundation grant to H.A. J.V. was supported by a grant from the Swiss National Foundation.

AUTHOR CONTRIBUTIONS

H.A. and S.P. conceived the study. S.P. performed all of the *in vivo* extracellular barrel cortex experiments. H.A. performed all of the *in vivo* patch experiments. A.N. performed all of the *in vitro* circuit-mapping experiments. J.V. performed all of the visual cortex experiments. G.T. collected all of the whisker tracking data and performed laminar boundary analysis. R.H., L.Y. and D.T. provided technical assistance. H.A. wrote the paper. A.N. and S.P. contributed equally to this study.

COMPETING FINANCIAL INTERESTS

The authors declare no competing financial interests.

1. Ramón y Cajal, S. *Histology of the Nervous System of Man and Vertebrates* (Oxford University Press, New York, 1995).
2. Gilbert, C.D. & Kelly, J.P. The projections of cells in different layers of the cat's visual cortex. *J. Comp. Neurol.* **163**, 81–105 (1975).
3. Thomson, A.M. & Lamy, C. Functional maps of neocortical local circuitry. *Front. Neurosci.* **1**, 19–42 (2007).
4. Feldmeyer, D. Excitatory neuronal connectivity in the barrel cortex. *Front. Neuroanat.* **6**, 24 (2012).
5. Lefort, S., Tomm, C., Floyd Sarria, J.C. & Petersen, C.C. The excitatory neuronal network of the C2 barrel column in mouse primary somatosensory cortex. *Neuron* **61**, 301–316 (2009).
6. Douglas, R.J. & Martin, K.A. Neuronal circuits of the neocortex. *Annu. Rev. Neurosci.* **27**, 419–451 (2004).
7. Binzegger, T., Douglas, R.J. & Martin, K.A. A quantitative map of the circuit of cat primary visual cortex. *J. Neurosci.* **24**, 8441–8453 (2004).
8. Malpeli, J.G. Activity of cells in area 17 of the cat in absence of input from layer a of lateral geniculate nucleus. *J. Neurophysiol.* **49**, 595–610 (1983).
9. Constantinople, C.M. & Bruno, R.M. Deep cortical layers are activated directly by thalamus. *Science* **340**, 1591–1594 (2013).
10. Mignard, M. & Malpeli, J.G. Paths of information-flow through visual-cortex. *Science* **251**, 1249–1251 (1991).
11. Armstrong-James, M., Fox, K. & Dasgupta, A. Flow of excitation within rat barrel cortex on striking a single vibrissa. *J. Neurophysiol.* **68**, 1345–1358 (1992).
12. Krupa, D.J., Wiest, M.C., Shuler, M.G., Laubach, M. & Nicolelis, M.A. Layer-specific somatosensory cortical activation during active tactile discrimination. *Science* **304**, 1989–1992 (2004).
13. Haider, B., Hausser, M. & Carandini, M. Inhibition dominates sensory responses in the awake cortex. *Nature* **493**, 97–100 (2013).
14. Niell, C.M. & Stryker, M.P. Modulation of visual responses by behavioral state in mouse visual cortex. *Neuron* **65**, 472–479 (2010).
15. Gradinaru, V. *et al.* Molecular and cellular approaches for diversifying and extending optogenetics. *Cell* **141**, 154–165 (2010).
16. Atasoy, D., Aponte, Y., Su, H.H. & Sternson, S.M. A FLEX switch targets Channelrhodopsin-2 to multiple cell types for imaging and long-range circuit mapping. *J. Neurosci.* **28**, 7025–7030 (2008).
17. Madisen, L. *et al.* A robust and high-throughput Cre reporting and characterization system for the whole mouse brain. *Nat. Neurosci.* **13**, 133–140 (2010).
18. Niell, C.M. & Stryker, M.P. Highly selective receptive fields in mouse visual cortex. *J. Neurosci.* **28**, 7520–7536 (2008).
19. Nowak, L.G., Azouz, R., Sanchez-Vives, M.V., Gray, C.M. & McCormick, D.A. Electrophysiological classes of cat primary visual cortical neurons in vivo as revealed by quantitative analyses. *J. Neurophysiol.* **89**, 1541–1566 (2003).
20. Agmon, A. & Connors, B.W. Correlation between intrinsic firing patterns and thalamocortical synaptic responses of neurons in mouse barrel cortex. *J. Neurosci.* **12**, 319–329 (1992).
21. Curtis, J.C. & Kleinfeld, D. Phase-to-rate transformations encode touch in cortical neurons of a scanning sensorimotor system. *Nat. Neurosci.* **12**, 492–501 (2009).
22. O'Connor, D.H., Peron, S.P., Huber, D. & Svoboda, K. Neural activity in barrel cortex underlying vibrissa-based object localization in mice. *Neuron* **67**, 1048–1061 (2010).
23. Diamond, M.E., von Heimendahl, M., Knutsen, P.M., Kleinfeld, D. & Ahissar, E. 'Where' and 'what' in the whisker sensorimotor system. *Nat. Rev. Neurosci.* **9**, 601–612 (2008).
24. Brumberg, J.C., Pinto, D.J. & Simons, D.J. Spatial gradients and inhibitory summation in the rat whisker barrel system. *J. Neurophysiol.* **76**, 130–140 (1996).
25. Helmstaedter, M., Staiger, J.F., Sakmann, B. & Feldmeyer, D. Efficient recruitment of layer 2/3 interneurons by layer 4 input in single columns of rat somatosensory cortex. *J. Neurosci.* **28**, 8273–8284 (2008).
26. Tarczy-Hornoch, K., Martin, K.A.C., Jack, J.J.B. & Stratford, K.J. Synaptic interactions between smooth and spiny neurones in layer 4 of cat visual cortex in vitro. *J. Physiol.* (*Lond.*) **508**, 351–363 (1998).
27. Bortone, D.S., Olsen, S.R. & Scanziani, M. Translaminar inhibitory cells recruited by layer 6 corticothalamic neurons suppress visual cortex. *Neuron* **82**, 474–485 (2014).

28. Feldmeyer, D., Roth, A. & Sakmann, B. Monosynaptic connections between pairs of spiny stellate cells in layer 4 and pyramidal cells in layer 5A indicate that lemniscal and paralemniscal afferent pathways converge in the infragranular somatosensory cortex. *J. Neurosci.* **25**, 3423–3431 (2005).
29. Feldmeyer, D. & Sakmann, B. Synaptic efficacy and reliability of excitatory connections between the principal neurons of the input (layer 4) and output layer (layer 5) of the neocortex. *J. Physiol.* (*Lond.*) **525**, 31–39 (2000).
30. Tamás, G., Buhl, E.H. & Somogyi, P. Fast IPSPs elicited via multiple synaptic release sites by different types of GABAergic neurone in the cat visual cortex. *J. Physiol.* (*Lond.*) **500**, 715–738 (1997).
31. Xiang, Z., Huguenard, J.R. & Prince, D.A. Synaptic inhibition of pyramidal cells evoked by different interneuronal subtypes in layer v of rat visual cortex. *J. Neurophysiol.* **88**, 740–750 (2002).
32. Packer, A.M. & Yuste, R. Dense, unspecific connectivity of neocortical parvalbumin-positive interneurons: a canonical microcircuit for inhibition? *J. Neurosci.* **31**, 13260–13271 (2011).
33. Gorski, J.A. *et al.* Cortical excitatory neurons and glia, but not GABAergic neurons, are produced in the Emx1-expressing lineage. *J. Neurosci.* **22**, 6309–6314 (2002).
34. Kätzel, D., Zemelman, B.V., Buetfering, C., Wolfel, M. & Miesenbock, G. The columnar and laminar organization of inhibitory connections to neocortical excitatory cells. *Nat. Neurosci.* **14**, 100–107 (2011).
35. Li, L.Y. *et al.* A Feedforward inhibitory circuit mediates lateral refinement of sensory representation in upper layer 2/3 of mouse primary auditory cortex. *J. Neurosci.* **34**, 13670–13683 (2014).
36. Gong, S. *et al.* Targeting cre recombinase to specific neuron populations with bacterial artificial chromosome constructs. *J. Neurosci.* **27**, 9817–9823 (2007).
37. Apicella, A.J., Wickersham, I.R., Seung, H.S. & Shepherd, G.M.G. Laminarly orthogonal excitation of fast-spiking and low-threshold-spiking interneurons in mouse motor cortex. *J. Neurosci.* **32**, 7021–7033 (2012).
38. Otsuka, T. & Kawaguchi, Y. Cortical inhibitory cell types differentially form intralaminar and interlaminar subnetworks with excitatory neurons. *J. Neurosci.* **29**, 10533–10540 (2009).
39. Ma, Y., Hu, H., Berrebi, A.S., Mathers, P.H. & Agmon, A. Distinct subtypes of somatostatin-containing neocortical interneurons revealed in transgenic mice. *J. Neurosci.* **26**, 5069–5082 (2006).
40. Oliva, A.A., Jiang, M.H., Lam, T., Smith, K.L. & Swann, J.W. Novel hippocampal interneuronal subtypes identified using transgenic mice that express green fluorescent protein in GABAergic interneurons. *J. Neurosci.* **20**, 3354–3368 (2000).
41. Royer, S. *et al.* Control of timing, rate and bursts of hippocampal place cells by dendritic and somatic inhibition. *Nat. Neurosci.* **15**, 769–775 (2012).
42. Fanselow, E.E. & Nicolelis, M.A. Behavioral modulation of tactile responses in the rat somatosensory system. *J. Neurosci.* **19**, 7603–7616 (1999).
43. Khatri, V., Hartings, J.A. & Simons, D.J. Adaptation in thalamic barreloid and cortical barrel neurons to periodic whisker deflections varying in frequency and velocity. *J. Neurophysiol.* **92**, 3244–3254 (2004).
44. Jiang, X.L., Wang, G.F., Lee, A.J., Stornetta, R.L. & Zhu, J.J. The organization of two new cortical interneuronal circuits. *Nat. Neurosci.* **16**, 201–2018 2013).
45. Helmstaedter, M., Sakmann, B. & Feldmeyer, D. Neuronal correlates of local, lateral, and translaminar inhibition with reference to cortical columns. *Cereb. Cortex* **19**, 926–937 (2009).
46. Priebe, N.J. & Ferster, D. Inhibition, spike threshold, and stimulus selectivity in primary visual cortex. *Neuron* **57**, 482–497 (2008).
47. Adesnik, H. & Scanziani, M. Lateral competition for cortical space by layer-specific horizontal circuits. *Nature* **464**, 1155–1160 (2010).
48. Hirsch, J.A., Alonso, J.M., Reid, R.C. & Martinez, L.M. Synaptic integration in striate cortical simple cells. *J. Neurosci.* **18**, 9517–9528 (1998).
49. Isaacson, J.S. & Scanziani, M. How inhibition shapes cortical activity. *Neuron* **72**, 231–243 (2011).
50. Ozeki, H., Finn, I.M., Schaffer, E.S., Miller, K.D. & Ferster, D. Inhibitory stabilization of the cortical network underlies visual surround suppression. *Neuron* **62**, 578–592 (2009).

ONLINE METHODS

All experiments were performed in accordance with the guidelines and regulations of the Animal Care and Use Committee of the University of California, Berkeley.

Transgenic mice. Mice used for experiments in this study were either wild-type (ICR white strain, Charles River), heterozygous for the scnn1-tg3-Cre allele (JAX stock # 009613), or heterozygous for drd3-Cre (strain KL196, MMRRC). A subset of mice carried the Ai9 Rosa-LSL-tdTomato allele (JAX stock # 007909) to help quantify the infection rate of Cre^+ cells. The scnn1-tg3-Cre and drd3-Cre lines were outcrossed several generations into the ICR white background to improve habituation to locomotion under head fixation. Mice used for visual cortical physiology were than backcrossed to C57/B6 mice for one generation to produce mice with pigmented eyes. For a subset of experiments in brain slices we used the emx1-IRES-Cre line (JAX stock #005628), PV-cre line (B6;129P2-$Pvalb^{tm1(cre)Arbr/J}$; JAX stock #008069), or the GIN line (FVB-Tg(GadGFP)45704Swn/J; JAX stock #003718). For *in vivo* experiments mice were between 4–8 weeks old. For labeling all inhibitory neurons we used GAD67-GFP mice[51]. To quantify the fraction of L4 excitatory neurons that express Cre, we analyzed slices from scnn1-tg3-Cre;GAD67-GFP mice injected with AAV-flexed-tdTomato and were counterstained for NeuN. We found that tdTomato+ cells in these mice constituted 85 ± 3% of excitatory L4 neurons. Mice were housed in cohorts of five or less with a light:dark cycle of 12:12 h, and were used for experimentation during their subjective night.

Viral infection. Neonatal scnn1-tg3-Cre mice (P3–6) were injected transcranially with ~20 nl of AAV9-DIO-ef1a-eNpHR3.0-YFP at three locations in S1 or V1. Viral infection at this age gave us reliable, dense and broad infection across most of either S1 or V1 and avoided toxicity we observed when injecting high titer AAV- eNpHR3.0 in adult mice. For *in vivo* ChR2 expression, AAV-2/1-DIO-Ef1a-ChR2-YFP was injected at P21–24. For in *vitro* experiments, neonatal scnn1-tg3-Cre, PV-cre, or emx1-cre mice were injected with AAV9-CAG-flexed-Chr2-tdTomato at P0-P4. Viruses were acquired from the University of Pennsylvania Vector Core. Undiluted viral aliquots were loaded into a Drummond Nanoject injector. Neonates were briefly cryo-anesthetized and placed in a head mold. With respect to the lamba suture coordinates for S1 were 2.0 mm AP, 3.0 mm L, 0.3 mm DV. For V1 they were 0.0 mm AP, 2.2 mm L, 0.3 mm DV.

Preparation for *in vivo* recording. Mice were anesthetized with isoflurane (2.5% vapor concentration). The scalp was removed, the fascia retracted, and the skull lightly etched with a 20 gauge needle. Following application of Vetbond to the skull surface, a custom stainless steel headplate was fixed to the skull with dental cement (Metabond). 2 d after surgery mice were habituated for 2–7 d to head-fixation on a free-spinning circular treadmill. On the day of recording mice were briefly anesthetized with isoflurane (2%), the skull over S1 or V1 was thinned, and a small (<250 μm) craniotomy was opened over S1 or V1 with a fine needle. In some cases S1 was previously identified with intrinsic optical imaging. The small size of the craniotomy ensured a stable preparation for both extracellular and intracellular recording.

Tactile stimulus presentation. While mice ran on the treadmill, they rhythmically swept their whiskers in a stereotyped manner (see **Supplementary Fig. 4**). To stimulate the whiskers a vertical metal bar (0.5-mm diameter) was rapidly (~50 ms) moved into the whisking field using a stepper motor with submicron precision (Oriental Motor) and controlled by digital signals (National Instruments PCIe-6353). The bar was presented at eight different positions, evenly spanning the entire rostral-caudal axis of the whisking field, in a randomly ordered sequence. An additional ninth position that did not contact the whiskers was used to compute non-contact evoked firing rates. The horizontal distance between adjacent stimulus positions was 2.2 mm, and controlled by moving the stepper motor on a linear stage with submicron precision (Zaber Technologies). Most mice habituated quickly to the presentation of the tactile stimulus assessed by lack of a change in whisking or running speed during stimulus presentation. Mice that did not habituate were excluded from this study. Mice were neither punished nor rewarded for any aspect of their behavior. Most mice ran consistently for hundreds of trials. In all cases we recorded from the C1-C3 or B1-B3 columns verified by a combination of intrinsic optical imaging and/or electrophysiology. Of eight stimulus positions, 3–5 contacted the principal whisker, and at each position, 2–3 whiskers contacted the stimulus, as assayed by separate experiments in which we tracked a single row of whiskers with high speed imaging. In a subset of mice, after physiological identification of the principal whisker, the surround whiskers were trimmed from the face to prevent contact with the object.

In the AAV-2/9-eNpHR3.0 experiments, five mice were used for recordings focused on collecting data from L2/3. In six separate mice, recordings focused on collecting data from L4 and L5, and in three additional mice, recordings focused on recording from L5 and L6. In the AAV-2/1-DIO-Ef1a-ChR2-YFP experiments, three mice were used to record across layers 2 through 5. In the YFP control experiments, two mice were used to collect data from layers 2 through 5.

Visual stimulation. Visual stimuli were generated with Psychophysics Toolbox running on a Mac Mini and were presented on a gamma corrected 23-inch Eizo FORIS FS2333 LCD display with a 60-Hz refresh rate. Stimuli consisted of drifting square wave gratings at 0.04 cycles per degree and 2 cycles per s of eight different directions (0–315° in steps of 45°) and either five different contrast levels (10–100% in logarithmic steps) or five different sizes (8, 13, 21, 36, 60 visual degrees), centered on the average receptive fields of all simultaneously recorded neurons. Gratings drifted for 2 s with 1-s inter-trial intervals with the red LED (Lumencor) switched on for 1 s starting 0.5 s after start of the visual stimulus in 50% of the trials. Suppression index was calculated as the difference between the peak response and the response to the largest stimulus, divided by the peak response $(FR_{PS} - R_{LS})/FR_{PS}$.

***In vivo* extracellular multi-electrode electrophysiology.** A 16- or 32-channel linear electrode (NeuroNexus, A1x16-3mm-25-177-A16 or A1x32-5mm-25-177-A32), or a subset of experiments a four shank 'Buzsaki32' style probe, was guided into the brain using a micromanipulator (Sutter Instruments) and a stereomicroscope (Leica). Electrical activity was amplified (A-M Systems), digitized at 30 kHz (National Instruments PCIe-6353), and stored on a computer hard drive. The cortical depth of each electrical contact was determined by zeroing the bottom contact to the surface of the brain. To ensure the electrode trajectory was close to perpendicular to the brain surface, the animal's skull was tilted relative to the vertically mounted electrode. After each recording a laminar probe coated with the lipophilic dye DiI was used to mark the electrode track and quantitatively assess insertion angle and depth. The laminar depth of recorded units was corrected for this insertion angle and the local curvature of the neocortex. In a subset of recordings we also assessed electrode depth by computing the current source density during sensory stimulation and identifying a sink corresponding to L4[18]. All three metrics (micromanipulator depth, DiI labeling, and CSD analysis) were in close correspondence (**Supplementary Fig. 2**). Laminar boundaries, consistent with published values[5], were measured from several lines of layer-specific Cre driver mice (scnn1-tg3-Cre, drd3-Cre, Rbp4-Cre and Ntsr1-Cre; **Supplementary Fig. 2**) cross to ROSA26-LSL-tdTomato.

Optogenetic stimulation *in vivo*. For optogenetic stimulation of eNpHR3.0 *in vivo* we used red light (30–80 mW mm^{-2}) from the end of a 1-mm diameter multimode optical fiber coupled either to a red laser diode (Ultralasers) or a solid state source (Lumencor Spectra X) controlled by analog and digital outputs (NI PCIe-6353). The fiber was placed as close to the craniotomy as possible (<3 mm). For activation of ChR2 we used blue light from a fiber coupled LED (Thorlabs). The illumination area was set to cover the entire macrovibrissal barrel cortex.

Analysis of multi-electrode neural data. Spike detection was performed using the UltaMega Sort package[52] in Matlab (Mathworks). After detection, spikes were automatically sorted into clusters of discrete units. Units were then manually sorted to meet criteria for inclusion while simultaneously preventing pseudo-replication. Quality metrics included analysis of spike amplitude, spike rate, auto-correlation, inter-spike interval, outlier removal, distance from threshold and cortical depth of largest waveform. With the exception of a small group of fast-spiking or burst firing units, included units had no more 1% of their individual waveforms violating a refractory period of 2.5 ms.

In sorted units mean firing rates were computed from counting spikes in a 550-ms window starting 200 ms after the onset of the red LED, and 700 ms after the onset of moving the bar into the whisker field. This window was chosen

because within 700 ms of the bar entering the whisker field, neuronal firing rates reached a stable steady-state. Trials containing stimulation periods where the animal's average running speed during the stimulus period deviated by more than 1.3 s.d. of its mean velocity were excluded, to ensure consistency in behavior across trials. The depth of each unit was assigned based on the calculated depth of the electrode on the array that exhibited its largest amplitude sorted waveform. Layer boundaries follow ref. 5 and were confirmed experimentally in a subset of recordings with current source density analysis[18] and histological assessment. CSDs were calculated from the trial-averaged local field potential (0.5–300 Hz) measured at each electrode contact, as previously published[53–55]. We estimated the layer 4/5 boundary as the base of the current sink corresponding to layer 4.

Statistically significant differences between conditions were determined using standard parametric or nonparametric tests, including a one-way or two-way ANOVA, Student's *t* test, and a Wilcoxon sign-rank test. Tests for normality were performed with a Lilliefors test. An optogenetic modulation index (OMI) for each condition was computed as the difference of the firing rates of a given unit between the light and no light condition, divided by their sum. Thus an OMI < 0 indicates suppression, OMI > 0 indicates facilitation, and OMI = 0 indicates no change. A small subset of L5 units (5/128, or 3.9%) displayed OMIs close to −1 indicating nearly complete suppression, and were statistical outliers. These neurons most likely correspond to a small subset of Cre^+ neurons in L5 that expressed eNpHR3.0, and were excluded from analysis.

The effect of layer 4 suppression on L5 sensory tuning was assessed using the following methods: an index of spatial tuning was calculated by dividing the firing rate at the peak of the tuning by the mean spike rate across all eight conditions (similar to a previous study that using this approach to measure angular tuning)[24]. Using this metric, a tuning index of one (STI = 1) indicates no preference for any stimulus, while a tuning index of eight (STI = 8) indicates a selective response to only one stimulus. The slope of a least-squares linear regression was used to determine how the effect of L4 suppression changed as a function of sensory drive. To calculate the full width at half max, a Gaussian function was fit to neuronal spatial tuning curves using the method of least-squares with upper and lower boundaries limited by the peak-evoked and spontaneous firing rate of each neuron, respectively.

Neuronal burst rate was calculated using a Poisson surprise method[56]. High-frequency spikes were counted as the number of spikes with at least one neighboring spike occurring in less than 10 ms. The coefficient of variation (CV) of interspike intervals (ISIs) was used to provide a quantitative description of spiking regularity. Bursting neurons have more irregular firing patterns, and are therefore characterized by a large CV. As the firing rate of a neuron approaches its refractory period, variation across trials necessarily decreases. Fano factor provides a reliable metric of this 'ceiling effect'.

Individual units were classified as either fast-spiking or regular spiking using a k-means cluster analysis of spike waveform components. One major component of waveform classification was the normalized difference between the two positive-going peaks. The other major component was the trough-to-peak latency of the large negative-going deflection. Fast-spiking units were categorized by a larger second positive-going peak (positive difference), and a short (less than 0.33 ms) trough-to-peak latency, following a previously established approach[57] (see **Supplementary Fig. 7a**,**b**). A subset of units on the border between the classification as FS or RS was excluded from analysis, although their inclusion did not change the significance of any results.

***In vivo* intracellular recording and analysis.** Mice were prepared identically as for extracellular recording. To make blind whole-cell patch-clamp recordings a glass borosilicate pipette (Sutter) was pulled to a long taper and a low resistance (3–5 MΩ) and inserted axially through the dura mater under high positive pressure. Electrode solution was the same as for brain slice recording for voltage clamp (see below, containing cesium, QX-314, and TEA). Signals were amplified with an Axopatch 200B (Molecular Devices), filtered at 2 kHz, and digitized with a National Instruments DAQ device (PCIe-6323).

The depth of the electrode was set to zero when the pipette encountered the dural surface, which was easily identified electrically by a large, transient increase in pipette resistance. The pipette was then advanced to L5 (~575–900 μm below the dura) under high pressure (~180 mbar). At the entry point of L5 pressure was quickly lowered to <30 mbar to search for neurons in the blind configuration. The pipette was advanced in 2-μm steps and following a sudden and transient increase in pipette resistance the positive pressure was released. Following gigaseal formation brief suction ruptured the membrane providing whole cell access. The cell was dialyzed for 2–3 min before obtaining data on synaptic excitation, and an additional 5–10 min before voltage clamping to the reversal potential of synaptic excitation to isolate inhibitory currents. Initial uncompensated access resistance averaged 17 ± 2 MΩ (range, 7–23 MΩ), and cells were excluded if this changed by more than 20% during the duration of the recording. Illumination trials were interleaved with control trials for all experiments to ensure that any slow drift in cell stability would not affect the results.

Excitatory and inhibitory synaptic charge was calculated as the integral under the current record at the corresponding apparent reversal potentials for GABA and glutamate. Most neurons exhibited a high rate of tonic synaptic excitatory and inhibitory currents. To calculate a baseline for charge measurements during sensory or optogenetic stimulation, current records for each trial were automatically scanned for a 50-ms period of the lowest variance during the second before the stimulus entry, and the mean of this interval was subtracted from the entire trace. Due to the high ongoing rate of inputs optogenetic suppression of L4 often resulted in a reduction below baseline of either inhibition in L5 RS cells (5 of 10 cells) or excitation in L5 FS cells (5 of 6 cells). Statistical significance of optogenetic changes in excitatory and inhibitory charge were assessed with a paired *t* test.

Putative FS neurons were identified either by the width of their spikes recorded in the cell-attached configuration before membrane rupture, or, in the absence of spikes, by the fast decay of spontaneous excitatory postsynaptic currents (sEPSCs; **Supplementary Fig. 7d**). Based on the decay kinetics of sEPSCs from intracellularly recorded FS neurons in brain slices, we were able to set a criterion of $\tau < 2$ ms for FS neurons (**Supplementary Fig. 7c**,**d**). Of the 16 intracellularly recorded neurons in this study used for analysis in **Figures 4** and **6** were classified as FS neurons based on these criteria, and all cells showing fast action potentials in cell-attached also exhibit fast decaying sEPSCs.

Brain slice recording and optogenetic stimulation. Acute thalamocortical slices were prepared from the left hemisphere 2-4 weeks later as previously described[47]. Slices were placed in a recording chamber and constantly perfused with oxygenated artificial cerebro-spinal fluid (NaCl 119 mM, KCl 2.5 mM, $MgSO_4$ 1.3 mM, NaH_2PO_4 1.3 mM, glucose 20 mM, $NaHCO_3$ 26 mM, $CaCl_2$ 2.5 mM) maintained at 32°. Slices were oriented with the caudal surface facing up in the recording chamber. Slices were visually inspected with epifluorescence to confirm dense, even expression of ChR2-tdTomato in L4 (scnn1-tg3-Cre experiments) or across the entire cortex (emx1-Cre and PV-cre experiments). Slices in which expression appeared faint or uneven were discarded. Slices were further inspected under 40× magnification to confirm that Layer 5 pyramidal cell apical dendrites stayed roughly parallel with the surface of the slice or receded slightly deeper as they progressed apically, otherwise the slice was discarded.

In a subset of scnn1-tg3-Cre experiments, we removed L2/3 before recording. While briefly visualizing L4 with epifluorescence, a fine blade was used to sever the slice below the border between L2/3 and L4. L2/3 was then completely separated from the lower layers and discarded. Multiple cuts were performed to ensure complete horizontal coverage of barrel cortex and surrounding regions. Generally this also removed one third to one half of the volume of L4 in recorded areas, but preserved the basal most regions of L4, as well as its descending axons. Recorded neurons did not appear noticeably unhealthy and could be recorded from for extended periods with stable resting membrane potentials and input resistances.

Whole cell recordings were performed using glass micropipettes (2-3M resistance) pulled on a Sutter P-1000 Micropipette Puller. For recording pyramidal cells, pipettes were filled with a Cs^+ based internal ($CsMeSO_4$ 135 mM, NaCl 8 mM, HEPES 10 mM, Na_3GTP 0.3 mM, MgATP 4 mM, EGTA 0.3 mM, QX-314-Cl 5 mM, TEA-Cl 5mM). For recording interneurons and for connectivity testing, pipettes were filled with a potassium gluconate based internal (K-gluconate 135 mM, NaCl 8 mM, HEPES 10 mM, Na_3GTP 0.3 mM, MgATP 4 mM, EGTA 0.3 mM). In some experiments, Alexa Fluor 488 Hydrazide (5 μM) or biocytin (1%, vol/vol) was dissolved into the internal solution to enable morphological recovery. Voltage recordings were not corrected for the junction potential, which was 13 mV. Series resistance was monitored with negative voltage steps during each trial, and was compensated up to 60%. Data were analyzed from

doi:10.1038/nn.4123

recordings in which series resistance was below 25M and did not change by more than 25% during the course of the experiment. Data were acquired and filtered at 2 kHz using a Multiclamp 700B Amplifier (Axon Instruments) and digitized at 20 kHz (National Instruments). All data were acquired using custom written MATLAB (Mathworks) software. Fast-spiking cells could be distinguished on the basis of their non-adapting response to current injection and short duration action potentials (**Supplementary Fig. 7**).

Photo-stimulation *in vitro*. Laser light was generated using a 1W 445-nm diode laser (Ultralasers) and routed via a liquid light guide into a CEL5500 digital micromirror device (DMD) (Digital Light Innovations). The projection from the DMD was then collimated and integrated into the light path of the microscope, before being focused onto the slice chamber using a 5× or 40× objective lens (Olympus). For Scnn1-tg3-Cre experiments, the DMD passively reflected, but not spatially modulate, light. Prior to photo-stimulation, infrared and epifluorescence images were captured using an IR-1000 CCD camera (DAGE-MTI) and imported into MATLAB. For mapping experiments, these images were used define the borders of a grid for photo-stimulation. For Emx1-cre experiments, this was an area extending from just below the L1-L2 border to upper layer 6 (~810–870 μm) and covering 2–5 columns laterally (~400 to ~1000 μm). For PV-cre experiments, the slice was rotated to achieve complete or nearly complete coverage of all cortical layers. The DMD was used to pattern light into a square region (30–40 μm on a side). Each stimulation site was spaced 25–30 μm apart from adjacent ones, resulting in some overlap of adjacent stimuli. During mapping, a 50-ms ramp of light (1.25 mW mm^{-2} final intensity) was applied to one of these regions at a time. Ramps minimize activation of fibers of passage[47]. Ten regions were stimulated per second in a serial, pseudorandom order, with 4 s breaks after every 10 s of mapping. Control experiments were performed using identical stimulation conditions while recording from $ChR2^+$ neurons in all layers. To account for the different excitability of PV neurons, for PV-cre mapping experiments were performed at ~20°, and light stimuli measured 50 μm to each side. Control experiments recording spiking from ChR2 expressing cells confirmed that this yielded comparable efficacy and precision to the photostimulation protocol used in Emx1-Cre experiments (**Supplementary Fig. 9c,d**).

All data were analyzed using custom written MATLAB software. For mapping experiments, the DC component was removed from traces by subtracting a down-sampled and median-filtered duplicate of the trace. Charge was calculated as the integral of the EPSC/IPSC during photostimulation and the subsequent 50 ms. Population maps were generated by first rotating the average map collected in each experiment in order to horizontally orient the laminar boundaries of the mapped area. Maps were next translated vertically to align the L4-L5 laminar boundary, and translated horizontally to align either the home column or the soma position of the recorded cell, before being averaged to yield a population map. Average values are expressed as mean ± s.e.m. Statistical tests were performed using the paired *t* test (latency data; **Fig. 5b**).

Paired recording connectivity testing. Experiments were performed in slices prepared from either PV-cre; Flex-TdTomato or GIN-GFP mice. We first targeted whole-cell recordings to a fluorescent L5 interneuron, and then subsequently recorded from one or multiple neurons in L4 of the same column. Monosynaptic connectivity was tested by driving spiking in L4 neurons using trains of 1.5-ms, 2-nA current injections, while monitoring EPSCs in a reporter-labeled cell in L5. Stimulation was repeated at least 15 times in all pairs tested. For PV-cre experiments, connections were tested by driving trains of three spikes in L4 cells at 10 Hz, though in connected pairs a single spike was sufficient to drive a robust EPSC. In contrast, excitatory synapses onto Martinotti cells exhibit high rates of failure on the first spike, but display facilitating EPSCs during trains of high-frequency firing[58]. We therefore tested connections onto GIN GFP+ cells by driving trains of ten spikes at 70 Hz in the presynaptic cell. As a positive control, we confirmed that we could use this protocol to observe monosynaptic EPSCs in GIN GFP+ cells by recording from pairs of L5 pyramidal neurons and L5 GIN GFP+ (data not shown). The distance between the somata of recorded cells was 122 ± 41 μm for L4-L5 GIN pairs, and 180 ± 39 μm for L4-L5 PV pairs. To perform statistical tests, we created a contingency table by categorizing L5 interneurons based on two criteria: cell-type (as established by genetic labeling) and whether or not that interneuron received at least one connection from L4. We then used Fisher's exact test on these categorical data. For further confirmation, we also fit a generalized linear mixed-effects model to our connectivity data. This model allowed us to account for the non-independence and varying amount of observations of connectivity onto each L5 interneuron, which would invalidate standard binomial tests. We found a statistically significant effect of cell type on connectivity rate (data not shown), corroborating our previous analysis.

Whisker imaging and automated tracking. A high-speed camera (Basler acA2000-340km) was placed below the running wheel; whiskers were imaged from below using a telecentric lens (Edmund Optics NT58-257) and a mirror angled at 45 degrees. Whiskers were backlit from above using high-powered diffused infrared LEDs (CMVision-IR200). High-speed videos were acquired with a framegrabber (Silicon Software) at 495 frames per s with a 100-μs exposure and were synchronized with electrophysiology data via external triggers. Whisker tracking was performed offline using Whisk[59] (Janelia Farms, Howard Hughes Medical Institute), which returned whisker angles and positions for every frame. Tracking data was further processed and analyzed using custom MATLAB scripts written to extract whisker contacts, set-point, amplitude, phase, and frequency. Whisker contacts were defined as the moment a whisker trace entered a user specified region of interest placed around the border of the stimulus bar. Contact accuracy was verified by watching a subset of videos from each experiment.

Statistics. All analyses were performed using MATLAB (Mathworks). The analyses performed were: two-way ANOVA, Student's *t* test, paired *t* test, Wilcoxon signed rank test, Kruskal-Wallis test, and Fisher's exact test. Where relevant, all tests were two-sided. Shapiro-Wilk and Kolmogorov-Smirnoff tests were used to formally assess normality of data in cases where parametric tests were used. No statistical methods were used to pre-determine sample sizes, but we collected sample sizes similar to those reported in previous publications[9,22,34]. Blinding was not used in this study. In experiments involving multiple different stimuli (visual/tactile stimulation in awake mice, or *in vitro* optogenetic mapping), different stimuli were randomly interleaved. Unless noted, all plots with error bars are reported as mean ± s.e.m.

A **Supplementary Methods Checklist** is available.

51. Tamamaki, N. *et al.* Green fluorescent protein expression and colocalization with calretinin, parvalbumin, and somatostatin in the GAD67-GFP knock-in mouse. *J. Comp. Neurol.* **467**, 60–79 (2003).
52. Hill, D.N., Mehta, S.B. & Kleinfeld, D. Quality metrics to accompany spike sorting of extracellular signals. *J. Neurosci.* **31**, 8699–8705 (2011).
53. Nicholson, C. & Freeman, J.A. Theory of current source-density analysis and determination of conductivity tensor for anuran cerebellum. *J. Neurophysiol.* **38**, 356–368 (1975).
54. Reyes-Puerta, V. *et al.* Spatial structure of spiking correlations in the barrel cortex of anesthetized rats. *J. Mol. Neurosci.* **53**, S6 (2014).
55. Reyes-Puerta, V., Sun, J.J., Kim, S., Kilb, W. & Luhmann, H.J. Large-scale neural assembly sequences evoked by sensory stimulation in the adult rat barrel cortex *in vivo*. *Acta Physiol. (Oxf.)* **210**, 66 (2014).
56. Legéndy, C.R. & Salcman, M. Bursts and recurrences of bursts in the spike trains of spontaneously active striate cortex neurons. *J. Neurophysiol.* **53**, 926–939 (1985).
57. Reyes-Puerta, V., Sun, J.J., Kim, S., Kilb, W. & Luhmann, H.J. laminar and columnar structure of sensory-evoked multineuronal spike sequences in adult rat barrel cortex *in vivo*. *Cereb. Cortex* **25**, 2001–2021 (2014).
58. Silberberg, G. & Markram, H. Disynaptic inhibition between neocortical pyramidal cells mediated by martinotti cells. *Neuron* **53**, 735–746 (2007).
59. Clack, N.G. *et al.* Automated tracking of whiskers in videos of head fixed rodents. *PLOS Comput. Biol.* **8**, e1002591 (2012).